Paper III

Atmospheric icing in a coastal mountainous terrain, measurements and numerical simulations, a case study

ATMOSPHERIC ICING IN A COASTAL MOUNTAINOUS TERRAIN. MEASUREMENTS AND NUMERICAL SIMULATIONS, A CASE STUDY

Cold Regions Science and Technology, Accepted subject to revision

Magne A. Drage
Geophysical Institute, University of Bergen/The University Center on Svalbard, Norway

Gard Hauge
Storm Weather Center AS
Bergen, Norway

ABSTRACT

Icing on structures occurs as rime ice, clear ice or wet snow deposit. Reliable forecasts of duration and intensity of this icing requires prognoses of standard meteorological parameters, in addition to more specific parameters such as the density (ρ_{LWC}) of cloud Liquid Water Content (LWC). Icing conditions on the mountain Brosviksåta (723 m a.s.l., 61º 2` N, 5º 9` E), on the western coast of Norway were investigated from March 21-24, 2003. A nonrotating vertical steel rod mounted on a scale was used to measure the accumulated ice load. Air temperature, relative humidity and wind were measured at three levels along the mountain slope. The maximum build-up of ice, in this case study, was measured to 4.5 kg on a 1 m high 0.14 m diameter rod. Comparison of measured ice-growth rate and calculated ρ_{LWC} gave a correlation coefficient of 0.85.

A mesoscale atmospheric model (MM5) has also been tested at a high horizontal resolution (1km) in order to evaluate its ability to reproduce weather conditions where freezing occurs. Comparison from the direct measurements and calculations, with results from MM5, gave 58% of the measured accumulated ice growth. Further studies of real-time cases on a real-time system at a coarser model resolution will reveal its capability for forecasting freezing events.

1. Introduction

Atmospheric icing has severe economical and technological consequences for human activities. It occurs frequently in sub arctic and artic climates as well as exposed locations at a certain height above sea level. Convincing evidence of its effects comes from the long list of human activities that have occasionally been disrupted, such as aircraft operations, telecommunication networks, power transmission lines, roads and railways (Poots, 2000). Icing directly onto structures occurs as rime ice, clear ice or wet snow deposit. Reliable icing forecasts require meteorological data of standard parameters such as air temperature, relative humidity, wind speed, wind direction and turbulence, in addition to more specific parameters such as median volume droplet size and liquid water content of the air masses concerned.

Daily weather conditions along the Norwegian coast are primarily dominated by large scale synoptical systems moving in from the west. Large variations in weather conditions occur over just a few kilometers due to the fjords and coastal mountains creating a complex topography that directly influences atmospheric circulation patterns. To give a realistic reproduction of weather conditions during icing events, a weather prediction model of high horizontal and vertical resolution is necessary. The mesoscale model MM5 version 3.6.3 applied in this study (hereafter MM5) is thoroughly tested under such conditions and is assumed to give a realistic representation of the atmospheric conditions during freezing events. MM5 is the most widely used atmospheric research model in the world. The development of this modeling system is continuous and improvements are made on a monthly basis. The quality of the MM5 forecasts has, through many studies of real-time forecasting systems, shown to be as reliable as other atmospheric models in most situations (Grell et al., 1994).

Several methods and physical models exist for estimating the flow pattern around constructions as well as the shape and formation of ice upon them. These methods and models have been mostly concerned with cylinders (Chaine and Skeates, 1974, Makkonen, 1984, 1996, Haldar et al., 1996). In the past, a number of experiments have been conducted to establish a relationship between atmospheric icing and measured standard meteorological parameters (e.g. Ahti and Makkonen, 1982, Makkonen and Ahti, 1995, Lott and Jones, 1998, Sundin and Makkonen, 1998). The limitations of these methods are that standard (routinely observed) meteorological parameters are necessary but have shown not to be sufficient to describe the icing process. Here, a new attempt of establishing a relationship between atmospheric icing and routinely measured meteorological data has been performed.

The first attempt of applying a numerical boundary-layer model to predict LWC for icing calculations was made by Vassbø et al. (1998). They used the HIRLAM (High Resolution Limited Area Model) over Finnish topography. This was however a study which used very coarse horizontal and, not least, vertical resolution. The horizontal resolution was 22 km by 5.5 km. The model had only 3 layers below 627 m, which reproduced the planetary boundary layer poorly.

The improvement of mesoscale weather prediction models of high horizontal and vertical resolution opens for the possibility of being able to forecast icing. It was important to establish a relationship between actual in-cloud icing and the output from a real-time mesoscale weather prediction model. The following task was therefore undertaken: the results from a real-time ice-monitoring system and the measurements of standard meteorological parameters at Brosviksåta (723 m a.s.l.) were compared with the MM5

numerical simulations of the weather conditions. In this study, MM5 applied 38 layers in the vertical, where 17 of them were placed in the lowest kilometer above the ground in order to reproduce realistic results in the boundary layer. Icing was measured using an ice scale mounted at the mountain peak, in addition to 4 weather stations at 3 different levels leading down to 325 m.a.s.l.. All stations measured air temperature, relative humidity, wind speed and wind direction. Data from a synoptic weather station located in the nearby area were also included in the measurement dataset.

2. Study site and data

2.1 *Measurement setup*

The mountain Brosviksåta (723 m a.s.l., 61º 2` N, 5º 9` E, see also figure 1) is situated to the south of the Sognefjorden outlet on the western coast of Norway. The mountain faces open sea within the sector SSW to NNW. This region is highly affected by the passage of frontal systems moving up the North Atlantic Ocean. Air masses related to these frontal systems are often humid and have air temperatures favorable for atmospheric icing (-15 < TºC < -1) during the winter season (November-April).
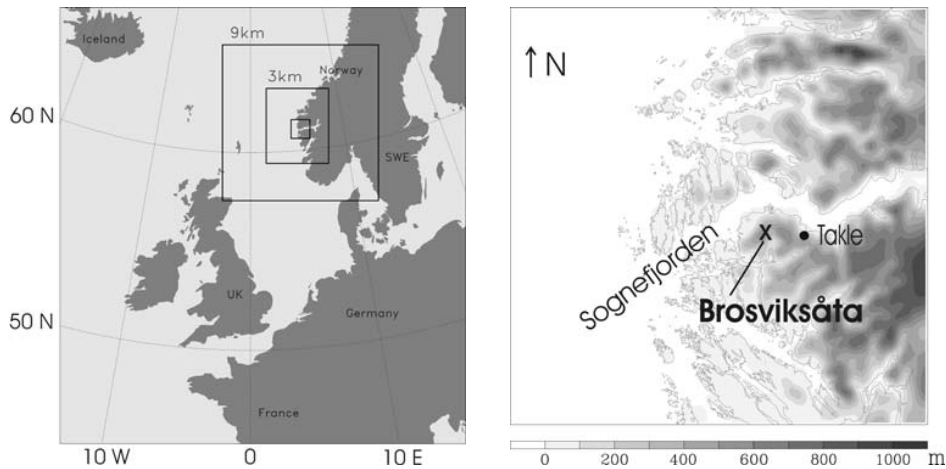

Figure 1. *Left figure shows the 3 nested MM5 domains within the European region with the Atlantic sea on the western boundary of the 9 km domain. The figure on the right hand side shows the 1 km MM5 topography along with the coastline. Brosviksåta is indicated on the figure with an X.*

The measurement setup consisted of four weather stations (two at 718 and one each at 520 and 325 m a.s.l.) and one ice scale (733 m a.s.l.). The weather stations were of the conventional type (Aanderaa Instruments, see http://www.aanderaa.com), consisting of a rotating cup anemometer for wind speed and a typical wind vane sensor for wind direction measurements. This equipment is not designed to operate during icing conditions. Nevertheless, an icing period could be detected from the time when the anemometer stopped rotating and the wind vane remained in a fixed position. Measurements from the site showed that the ice accumulation started at 1100 hrs March 21, while the two anemometers at the mountain top stopped rotating at 1750 hrs and 1820 hrs, respectively. In addition, air temperature and relative humidity were measured at all levels. The accuracy of the air temperature and relative humidity measurements are ±0.1C° and ±2%, respectively. The observation interval for all the weather stations was 10 minutes. In addition, precipitation data from the synoptic station Takle (38 m a.s.l.), situated 12 km east of the mountain base, are included. This station is operated by the Norwegian Meteorological Institute.

Icing was measured by an ice scale, consisting of a 1 m high vertical nonrotating steel rod of 14 cm diameter, measuring ice loads of up to 150 kg. A laboratory calibration test of the ice

scale system gave a precision and standard deviation of 0.1 kg and 0.027 kg, respectively (Drage and de Lange, 2004). This scale, with a logging interval of 10 minutes, was mounted 10 meters above the ground on the roof of a building (figure 2). The effect of the building on the ice scale was estimated to be negligible. Using a two month record at Mt. Brosviksåta with no icing, the precision of the instrument was found to be within the range of the laboratory test. During that period the wind speed reached more than 20 m/s.

Figure 2. *Ice scale mounted at Mt. Brosviksåta. The length of the cylindrical rod is 1 m and the diameter is 14 cm.*

2.2 *Weather prediction model*

The atmospheric mesoscale model MM5 was developed by PSU (Pennsylvania State University) and NCAR (National Centre for Atmospheric Research). It is a mesoscale modeling system that includes advanced atmospheric physics. It is widely used for real-time weather forecasts, air quality investigations and hydrological studies (Warner et al., 1991,

1998, Grell et al., 1994, Mass and Kuo, 1998, Chatfield et al., 1999, Chang et al., 2000, Mass et al., 2002). MM5 is based upon a set of equations for a fully compressible and non-hydrostatic atmosphere. Consequently it is possible to run the model at fine horizontal and vertical scales corresponding to the meso γ-scale (O(1)km).

Initial and lateral boundary conditions were obtained from the European Centre for Medium-Range Weather Forecasting (ECMWF) model with 0.5 degree distance between the grid points, and nested down to 9 km, 3 km and finally 1 km (figure 1). 38 vertically unevenly spaced full-sigma levels were placed in the vertical, with the highest density in the lowest 1500 meters. This allows the planetary boundary layer to be well represented in the model. MM5 was initiated as a "cold start" with no pre-forecast spin up period or assimilation of additional observations. This could however easily have been done, but observations are already assimilated into the analysis provided by the ECMWF, and we do not wish to use the same observational background data twice. By experience, the assimilation of observations would not have any large effect in this situation because conventional observation sites are sparse both in time and space during the time studied here.

MM5 has a wide variety of different options for the parameterization of sub-grid processes (Grell et al., 1994). Here, we have applied the turbulence scheme based on Hong and Pan (1996), coupled with a simple soil diffusion model. For moisture, an explicit scheme was applied, including super cooled water, ice, rain, snow and vapor (Reisner et al., 1998). Cumulus parameterization based on Kain and Fritsch (1993) was used for the 9 km domain, but not for the 3 km and 1 km domains. Topography and land-use were derived from the 1 km USGS (United States Geological Survey) dataset (Eidenshink and Faundeen, 1998). Finer topography grid was available from Norwegian sources. However, in this study the horizontal grid distance in the MM5 model was 1 km. A higher resolution would only have been smoothed to a 1 km model topography. Regarding the limitations of the physical sub-grid parameterizations, the 1 km resolution is seen as the present day limit of the MM5 system. Further information on the model system can be found in Grell et al. (1994).

3. Methods for calculating in-cloud icing

The rate of icing (dM/dt) onto an object is given by the equation

$$\frac{dM}{dt} = \alpha_1 \alpha_2 \alpha_3 \cdot \rho_{LWC} \cdot A \cdot V \qquad [\text{Kg} \cdot \text{s}^{-1}] \qquad (1)$$

where ρ_{LWC} is the density of liquid water content of the air, flowing with the wind velocity, V, towards the cross-sectional area, A, of the object. Efficiency coefficients α_1, α_2 and α_3 represent processes that reduce the rate of icing (Brun et al., 1955, Lozowski, 1983, Makkonen and Stallabras., 1987, Finstad et al., 1988). These factors vary between 0 and 1.

3.1 *Efficiency coefficients*

α_1 represents the collision efficiency of the particles, i.e. α_1 is the ratio of the flux density of the particles that hit the object to the flux density of particles in the cross sectional area upstream of the object. The collision coefficient α_1 becomes less than one when the water droplets moving towards an object follow the streamlines around it without colliding. Small droplets, large objects and low wind speeds reduce α_1. Langmuir and Blodgett (1946), and Finstad et al. (1988) conducted a theoretical investigation of water droplet trajectories around cylinders. This investigation describes how droplets hit the cylinder within a band limited between polar angles $-\varphi$ and φ (Figure 3). The angle φ_0 is a function of the droplet radius,
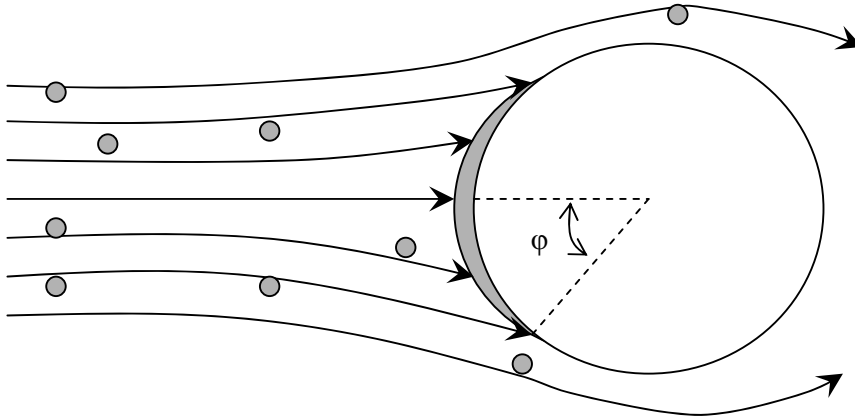
Figure 3. *Air streamlines of droplet trajectories around a cylindrical object*

cylinder radius, air speed, air temperature, and pressure. The equations are empirically fitted to the results of the collision efficiency, as given by Finstad et al. (1988) and Makkonen and Stallabras (1987). Here, collision efficiency is taken as being a function of median volume droplet diameter, wind speed and cylinder diameter. Variation of the collision efficiency is considerable. This theory is only valid for cylinders, which often makes it inapplicable in nature. Therefore, this theory of estimating the collision efficiency is limited to be valid only in the beginning of the ice incident discussed here. During time, the ice will form a vane against the wind, in which case the theory for a cylinder becomes inapplicable.

α_2 represents the efficiency of collection of those particles that hit the object, i.e. α_2 is the ratio of the flux density of the particles that stick to the object to the flux density of the particles that hit the object. The collection efficiency, α_2, is reduced from one when the particles begin to bounce from the surface. Particles are considered to have stuck either when they are permanently collected or when their residence time is sufficient to have affected the icing rate. As an example, the icing rate can be affected when there is heat exchange between surface and particle. The collection efficiency is assumed equal to 1 for in-cloud icing (Ahti and Makkonen, 1982).

α_3 represents the efficiency of accretion, i.e. α_3 is the ratio of icing to the flux density of the particles that stick to the surface. The heat released by freezing depends on the wind speed, ρ_{LWC}, as well as droplet size and diameter of the object. The efficiency of accretion reduces from 1 when the heat flux from the accretions is too small to cause sufficient freezing to incorporate all sticking particles into the accretion. In such a case, part of the mass flux of the particles is lost from the surface by run-off (Makkonen, 1996). At some specific ρ_{LWC} or wind speed the released heat of freezing will increase the surface temperature (T_s) to 0°C. The minimum value of ρ_{LWC} at which T_s reaches 0°C is called the Ludlam limit (Ludlam, 1951). T_s can be found iteratively by solving the equation of the heat balance over an ice surface, given by Mazin et al. (2001). However, this shedding of water from the surface is

7

often ignored when the air temperature is below 0ºC (Sundin and Makkonen, 1998). Thus, α_3 is set equal to 1 in this case study.

As the wind direction was nearly constant for this case study, the cross sectional area of the cylinder was assumed to be constant. The super cooled cloud droplets only hit the cylinder on the windward side, creating an ice vane facing the wind. This has been confirmed by visual observation. No measurements of droplet size were performed during the case study. Therefore, by assuming that the number of droplets per volume was constant, the droplet size is only correlated to the estimated ρ_{LWC}. From equation 1, the collision coefficient can be found using the observed ice-growth rate and estimates for wind speed and ρ_{LWC}:

$$\alpha = \frac{\left(dM/dt \right)}{A \cdot V \cdot \rho_{LWC}} \tag{2}$$

Observations show that the collision coefficient during icing varies from approximately 0.04 to 0.13 in this case study (figure 4), with the exception of the high values in the beginning of the period, which were associated with precipitation.
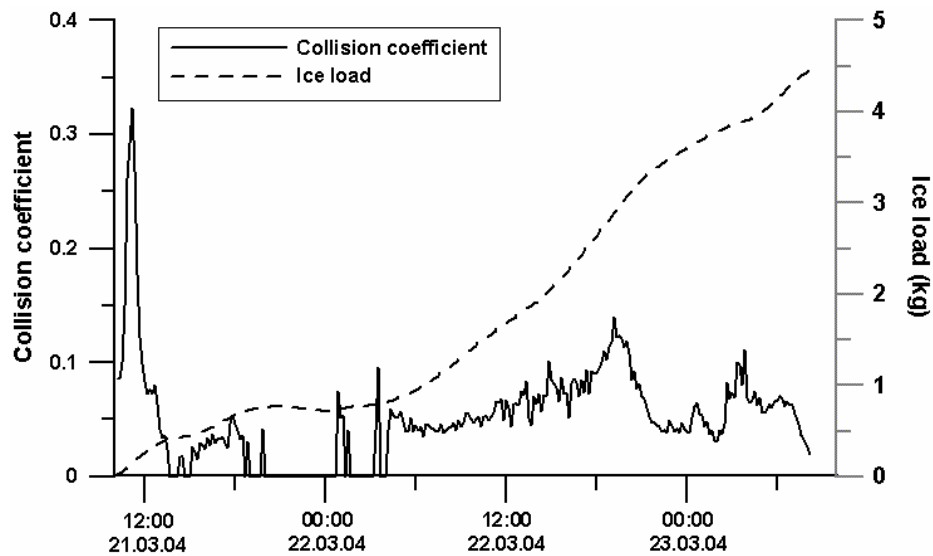

Figure 4. *Measured ice load and calculated collision coefficient based on equation 2, during the icing incident March 21 – 24 2003.*

3.2 Determination of cloud base and air temperature

Reliable values for air temperature and humidity are needed for estimation of water vapor pressure and density of dry air at certain heights above sea level. Measurements do not normally exist at any actual icing site, making reliable estimates of air temperature crucially important. A lifted volume of air close to the slope of the mountain is mixed with ambient air. However, this process is assumed to be near adiabatic. Air temperature at different heights for the volume of air that is lifted is assumed to follow the function;

$$T(z) = T_1 - \gamma_d \cdot (z - z_1) \qquad\qquad ;z \leq z_c \qquad\qquad (3.a)$$

$$T(z) = T_1 - \gamma_d \cdot (z_c - z_1) - \gamma_w \cdot (z - z_c) \qquad ;z > z_c \qquad (3.b)$$

where T_1 is the temperature at the lower station, z_1 and z_c is the height of the lower weather station and the cloud base, respectively. γ is defined as $-dT/dz$, where γ_d is the temperature gradient for unsaturated conditions (below cloud base) and γ_w is the temperature gradient for saturated conditions (inside the cloud). Earlier work suggests $\gamma_w = 0.54$ ºC/100m and $\gamma_d = 0.85$ºC/100m (Harstveit, 2002). Estimates from measurements at Brosviksåta suggest $\gamma_w = 0.62$ºC/100m and $\gamma_d = 0.92$ ºC/100m, with standard deviations of 0.07 and 0.08, respectively (figure 5).
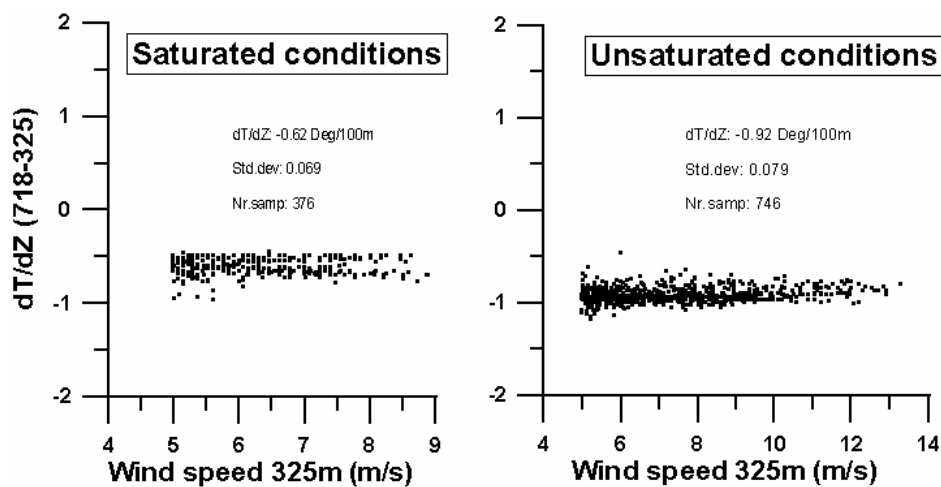

Figure 5. Measured temperature gradients for saturated (left) and unsaturated (right) conditions for wind speed above 5 m/s, wind direction in the sector 180 – 45 Deg. Besides average gradients (dT/dz), standard deviations and number of samples (Nr. Samp.) are given.

To exclude situations of high stability and weak mixing in the boundary layer, a lower wind speed limit of 5 m/s at the weather station at 325 m a.s.l. was chosen. Furthermore, only wind directions between South (180º) via North to East (45º) were chosen due to large scale turbulence created by the topography in the sector 45º – 180º degrees. Based on these criteria the value of 0.92 ºC/100m for unsaturated conditions indicates a slightly stable boundary layer, with a vertical temperature gradient less than adiabatic. This is consistent with

9

previous observations of a smaller increase in ρ_{LWC} with height than the adiabatic (Nicholls, 1984, Noonkester, 1984).

Before the temperature gradients defined above can be used, the height of the cloud base must be determined. The air temperature and pressure at the lower level 1 are T_1 and p_1, respectively, with mixing ratio w_1. This air is cooled by lifting at the temperature gradient for dry conditions, γ_d (defined above), until its adiabat intersects the vapor line defined by $w_s = w_1$. The air temperature at this level is T_c. An analytical approximation for T_c, which must be solved by iteration, is given by:

$$T_c = B / \ln\left[\frac{A\varepsilon}{wp_1}\left(\frac{T_1}{T_c}\right)^{1/k}\right] \tag{4}$$

where A, B, k are constants, respectively $2.53 \cdot 10^8$ kPa, $5.42 \cdot 10^3$ K and 0.286 (Rogers and Yau, 1989). w, T_1, and p_1 are known at the unsaturated lower level 1. T_c is therefore the air temperature at cloud base. Cloud base height is estimated by using the temperature gradients in equation 3 above, either by following the gradient for unsaturated conditions from below (3a), or by following the gradient for saturated conditions from above (3b).

$$z_c = \frac{T_1 - T_z + \gamma_d \cdot z_1}{\gamma_d} \qquad ; z_c > z_1 \quad (5a)$$

$$z_c = \frac{T_1 - T_z + \gamma_w \cdot z_1}{\gamma_w} \qquad ; z_c < z_1 \qquad (5b)$$

Equation 5a can be used during unsaturated conditions, and equation 5b during saturated conditions.

3.3 *Cloud liquid water content*

Mixing ratio w is defined as the mass of water vapor (M_v) per unit mass of dry air (M_d);

$$w = \frac{M_v}{M_d} = \frac{\rho_v}{\rho_d} \approx \varepsilon \cdot \frac{e}{p} \tag{6}$$

where p is the air pressure, e is the water vapor pressure, ρ_v is the water vapor density, and ρ_d is the density of dry air. ε is the constant ratio of the molecular weight for water vapor and dry air, equal to 0.622. The saturation vapor pressure e_s can be fitted to within 0.1% over the temperature range $-30°C \leq T \leq 35°C$ by the empirical formula

$$e_s(T) = 6.112 \exp\left(\frac{17.67 \cdot T}{T + 243.5}\right) \tag{7}$$

where e_s is in mb and T in degrees Celsius (Bolton, 1980).

The mixing ratio defined above is constant with height for a volume of air that is lifted dry adiabatically without any entrainment. In our case, measurements show that the temperature gradient for dry conditions at Brosviksåta is 0.92 °C/100m, while the dry adiabatic temperature gradient, $\Gamma = g/c_p = 0.98/100m$. This gives a difference in the temperature gradients of only 0.06 °C/100m, and the mixing ratio along the mountain slope is therefore assumed to be constant with height. This gives the relationship;

$$w_1 = \varepsilon \frac{e_1}{p_1} = w_2 = \varepsilon \frac{e_2}{p_2} \tag{8}$$

where the indices 1 and 2 refers to the lower (1) and the upper (2) levels, respectively.

10

A reduction in the mixing ratio at level 2 indicates saturation with respect to water vapor. Based upon the assumption that the total water content of the air is constant with height, the total mixing ratio, w_{tot}, is the sum of the saturation mixing ratio (w_s) and the liquid water content mixing ratio (w_{LWC}) at level 2, i.e.:

$$w_{s2} = w_{tot} - w_{LWC2} \qquad (9)$$

The total mixing ratio equals the mixing ratio at unsaturated conditions, in this case at the lower level 1:

$$w_{tot} = w_1 \qquad (10)$$

That means no fall out by rain and no exchange of water vapor between the air masses and the slope of the mountain.

Combining equation (8), (9) and (10) gives the mixing ratio of LWC at level 2:

$$\frac{\rho_{LWC2}}{\rho_{d2}} = w_1 - w_{s2} \qquad (11)$$

Combining equation (6) and (11) gives ρ_{LWC} in a cloud given by the equation

$$\rho_{LWC2} = \varepsilon \cdot \rho_{d2} \left(\frac{e_1}{p_1} - \frac{e_2}{p_2} \right) \qquad (12)$$

with the cloud base lying between the lower (1) and upper (2) level. Below the cloud base, at level 1, water in the air consists only of water vapor. Inside the cloud, at level 2, the water in the air consists of a mixture of water vapor and cloud liquid water.

Liquid water content of stratus clouds is usually in the range of 0.05 to 0.25 g/m^3, while in stratocumulus and deep nimbostratus the values are usually lower than 1 g/m^3 (Rogers and Yau, 1989). Detailed observations of the microphysical structures of marine stratus clouds (Nicholls, 1984, Noonkester, 1984), which are of importance in this case study, show average liquid water content over horizontal layers increasing with height, but with values less than adiabatic. This increase of water content with height is accounted for by an increase in droplet size rather than concentration of cloud drops. This is due to the fact that the growth process is dominated by condensation rather than coalescence. Because of this, the droplet spectrum in stratus clouds is relatively narrow, as expected with growth by condensation.

3.4 Wind speed estimates
Wind speed measurements were carried out along the slope of Brosviksåta at 325, 520 and 718 m a.s.l. Observations of wind speed were taken 2 meters above the ground, and given as 10 minute mean values. The wind sensors used were rotating cup anemometers, which stopped rotating when icing took place. The wind speed ratio between level 2 and level 1, (V_2/V_1) as a function of a lower limit of wind speed at level 1, was analyzed.

A data selection was performed with respect to air temperature, wind direction and wind speed. The air temperature must be higher than +1.5 ºC at 718 m a.s.l. to exclude all the icing incidents. The wind direction was in the sector 160 – 180 degrees (SSE–S) at the lower weather station at 325 m a.s.l. for the actual icing incident investigated in this case study. Based on one year of data collection at the site, with the wind direction and air temperature limits specified above, the results are shown in figure 6. This shows that the ratio decreases with increasing wind speed at 325 m a.s.l. from 2.25 at wind speed 4 m/s to 2.0 at wind speed 11-12 m/s. In this work, a lower limit of 5 m/s was chosen for level 1, which gives a ratio equal 2.2 and a standard deviation of 0.41.
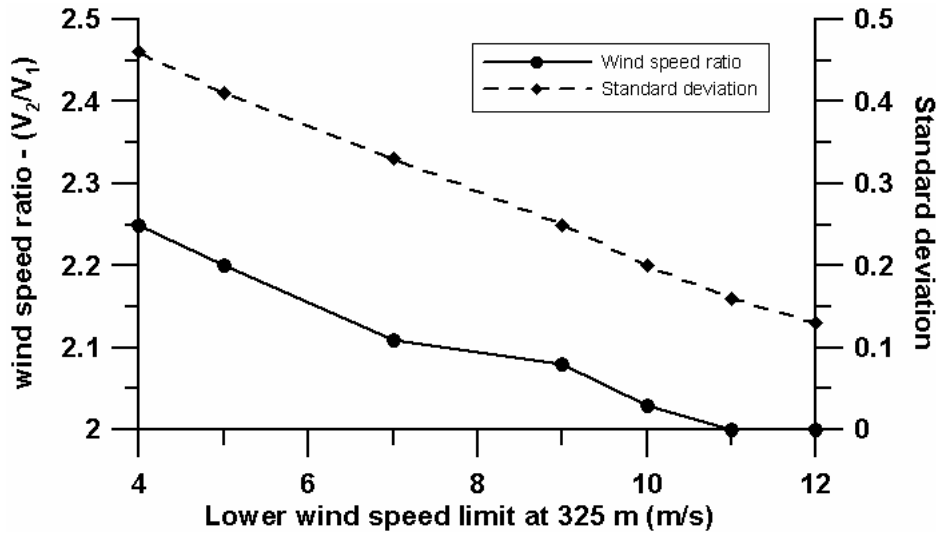
11

Figure 6. *Wind speed ratio, (left y-axis) and the standard deviation (right y-axis) as a function of wind speed at the lower level, with wind direction in the sector 160-180˚.*

4 Results and discussion

4.1 *Measurements and calculation of atmospheric ice accretion*

The icing incident in this study took place March 21-24 2003, with a maximum build-up of ice measured to approximately 4.5 kilograms (figure 7). In the beginning of the period, the air temperature was -3ºC with a near linear increase until it reached 0ºC on March 23. A sudden drop in ice load at the end of the period can be explained by the increase of temperature above 0ºC. The rate of precipitation was estimated from the synoptic weather station Takle, situated 12 km to the east of the mountain base, with measurements taken at 0600hrs and 1800hrs daily. Precipitation accumulated during the icing incident was 6.3 mm, with only three observed periods of precipitation (figure 7).

The first period of precipitation measured at Takle, from 0600hrs to 1800hrs March 21, was associated with a fast increase in ice load. This indicates that the ice load might have been a combination of in-cloud icing and precipitation icing. The ice load increases further by approximately 3 kilograms during the period from 0600hrs March 22 to 0600hrs March 23, when no precipitation was recorded. This period was therefore assumed only to be an in-cloud icing incident. An increase in air temperature above 0ºC at the mountain top as well as precipitation during the period 0600hrs to 1800hrs March 23 was associated with a sudden decrease in ice load due to melting and ice falling off from the scale.

The ρ_{LWC} in figure 7 was determined by Eq. 12 using the data recorded automatically by the weather stations along the mountain slope. Negative values in the beginning of the period were probably caused by low wind speeds and therefore a boundary layer that was not well mixed. Wind speed increases as the frontal system approaches. The method for determining the ρ_{LWC} given by Eq. (12) can therefore be applied.

A plot of the ice growth and the ρ_{LWC} during the icing incident from 0800 hrs March 21 until maximum ice load was reached on March 23 shows a good correlation of the two independently measured values (figure 7). The only exception is found in the beginning of the icing period. This can be explained by the fact that precipitation occurred in the same period, and the ice load was therefore a combination of in-cloud ice and precipitation ice. Decreasing ice growth rate towards zero around 2400 hrs March 22 was associated with the decreasing ρ_{LWC} (until it reached zero). Likewise, the decrease in ρ_{LWC} at around 0400 hrs
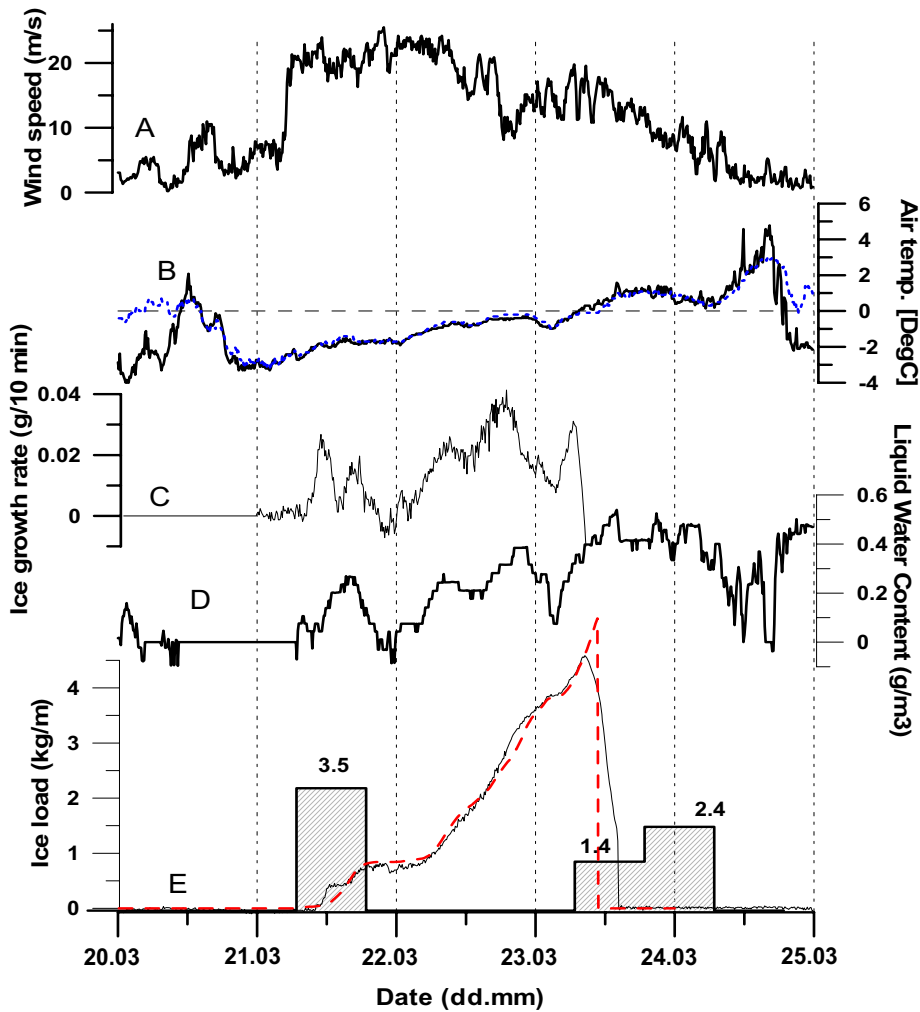

Figure 7. *A) Wind speed calculated at 723 m a.s.l. B) Air temperature estimated (solid line) and measured (dotted line) at 723 m a.s.l. C) Ice growth rate (g/m 10 min) 3 hrs running mean at the ice scale. D) Estimated liquid water content at 723 m a.s.l. E. Ice load measured (solid line) and estimated (dotted line) (kg/m) at the ice scale. Lower step plot shows 12 hrs accumulated precipitation, where the numbers above indicate the amount of precipitation in*

March 23 was associated with a decrease in ice growth rate at the same time. A statistical correlation between the ice growth rate and the ρ_{LWC}, from the beginning of the ice growth until it reached maximum weight, gives a correlation coefficient of 0.73. By excluding the period in the beginning, associated with precipitation, a higher correlation coefficient of 0.85 is found.

Ahti and Makkonen (1982) and Sundin and Makkonen (1998) estimate the in-cloud ice load, M_i (N m^{-1}), for each icing events as,

$$M_i = 5.5 \cdot 10^{-3} v_i T_i g \qquad (13)$$

where $5.5 \cdot 10^{-3}$ is an empirical constant, v_i is the wind speed (m s^{-1}) at the level of interest, T_i is the event duration (hrs), and g is the acceleration of gravity. Furthermore, the criteria for in cloud icing to occur is simply that the height of cloud base is lower than the height of interest and an air temperature in the range 0 to –15 °C. According to this theory, in-cloud icing intensity (kg m^{-1} s^{-1}) is independent of ρ_{LWC}. As mentioned above, however, measurements and calculations of the icing incident at Mt. Brosviksåta indicate a strong correlation between the ice growth rate and ρ_{LWC} (figure 7). This may also indicate a relationship between the ρ_{LWC} and the collision efficiency. Assuming collision efficiency equal to zero when ρ_{LWC} is zero and a linear increase of the collision efficiency creating an ice load equal the measured ice load at the end of the icing period, the following formula is obtained:

$$\alpha_1 = 0.225 \cdot \rho_{LWC} \qquad (14)$$

where ρ_{LWC} is in (g m^{-3}). The ice growth is assumed to stop when the air temperature reaches 0ºC. This result indicates a strong connection between the measured and calculated ice growth based on a collision efficiency determined only by the ρ_{LWC} (figure 7). This simple model for estimating the collision efficiency ignores the effects of changes in wind speed, shape and area of cylinder as well as the number of droplets per volume air. The independence of wind speed is explained by the fact that the wind speed is approximately constant during the icing incident studied here (figure 7). Further testing against similar cases of in-cloud icing is needed in order to verify the reliability of this model.

4.2 *MM5 results*

A qualitative evaluation of the data from the MM5 model run during the icing incident was performed. The modeled synoptic situation given by the MM5 model corresponded well with the observed weather data during the period in question. Wind speeds and temperatures in MM5 corresponded well with the observations near Brosviksåta as well as the synoptical observations at Takle. Main surface winds came from S to SW, with winds from W to NW in the higher model levels (500 – 700 hPa). At the same time, the model gives little or no precipitation during this period, though the cloud base was below the mountain top at Brosviksåta.The model performs a smoothening of the topography. This is why the ground level in the model was at a different level to the actual terrain in the area. Maximum height

of the mountain was found to be 554 m a.s.l. in the model topography at 1 km resolution (see also figure 1) whereas the actual height of the mountain is 723 m a.s.l. A correction of model data from 554 m a.s.l. to 723 m a.s.l. was necessary for determining icing. The modeled air temperature at the top of the mountain was found by following the temperature gradient for saturated conditions, found equal to $\gamma_w=0.62$, from 554 m up to 723 m (figure 8). It can be observed that the simulated air temperatures show a good correlation with the measured air temperatures, with an increase from -3 ºC in the beginning of the period until it reached +1 ºC at the end of the period. The model slightly underestimates air temperature, with an average error of 0.45 ºC. The correlation coefficient between measured and simulated air
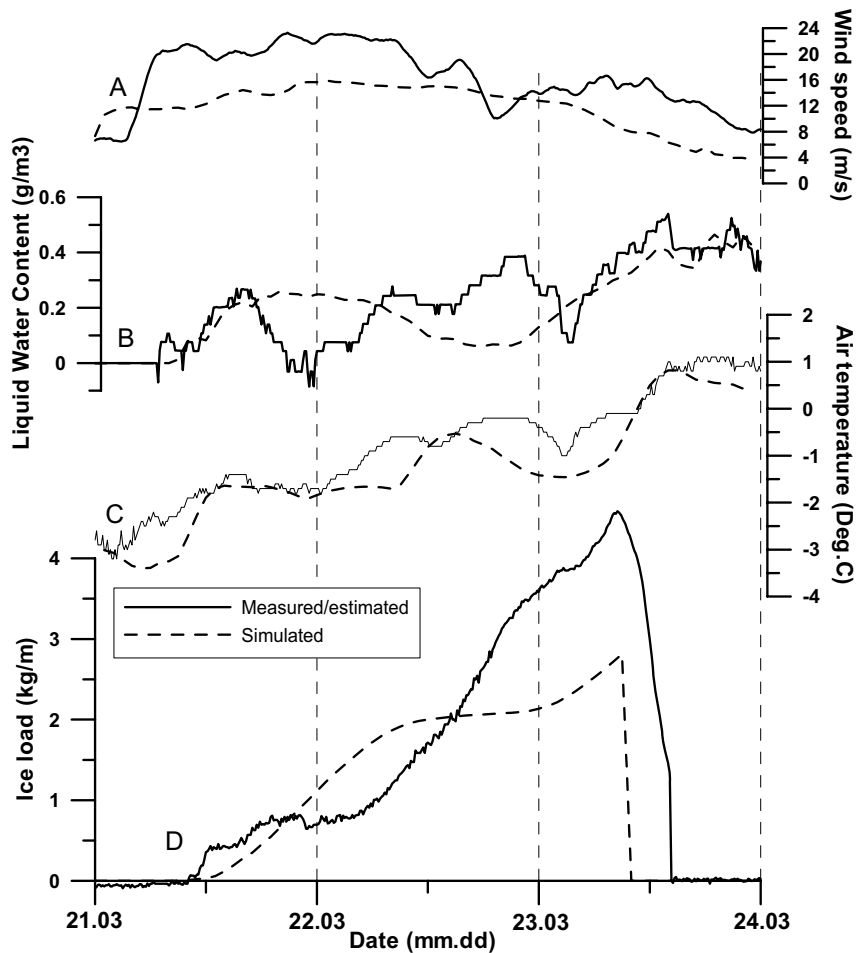

Figure 8. A) Wind speed and B) LWC estimated from measurements (solid line) at 723 m a.s.l and simulated by MM5 (dotted line) at 554 m a.s.l., respectively. C) Air temperature at 723 m a.s.l. measured (solid line) and simulated (dotted line). D) Ice load measured by the ice scale (solid line) and simulated by MM5 (dotted line).

temperatures is 0.94 in this case study.

ρ_{LWC} estimated from MM5 results and from the measurements during the icing incident are also given in figure 8. The model gave data at one-hour intervals. The surface effects on the model results at 723 m a.s.l. were significantly reduced by the smoothening of the topography in MM5. A model height of 554 m a.s.l. was therefore used for the ρ_{LWC}. Due to this, it has been assumed that the ρ_{LWC} was underestimated when the height was kept to 554 m a.s.l. Data from the MM5 model gave a ρ_{LWC} in the same size of order as the ρ_{LWC} determined from measurements (figure 8). As expected, MM5 slightly underestimates the ρ_{LWC}, with an average difference of 0.05 g/m^3. The correlation coefficient of these ρ_{LWC} values equaled 0.72.

Simulated ice growth was calculated by use of Eq. 1. α_2 and α_3 were set equal to one, and α_1 was estimated by Eq. 14, as in chapter 4.1 above. Values of ρ_{LWC}, wind speed and temperature were taken from the results of the MM5-simulation. According to figure 8, the simulated ice growth was underestimated, which may be addressed to the underestimation of the ρ_{LWC}.

5 Summary and conclusions

Reliable forecasts of duration and intensity of icing on structures as in-cloud ice requires data of standard meteorological parameters, in addition to more specific parameters such as the density of the liquid water content of the air (ρ_{LWC}). Icing conditions on the mountain Brosviksåta (723 m a.s.l., 61º 2` N, 5º 9` E), at the western coast of Norway was investigated in the period March 21-24, 2003 in this study. Measurements of ice growth on a one meter high non-rotating steel rod, of 0.14 m diameter, at the mountain peak showed a maximum build-up of 4.5 kg during that period. The type of icing was identified as mainly in-cloud icing by dry growth (rime ice), due to the fact that little precipitation was measured during the case study period.

A method for calculation of ρ_{LWC} has been described. The method only requires measurements of air temperature, air humidity and wind speed at a known level under unsaturated conditions. These parameters were measured at three different levels along the slope of the mountain. The beginning and end of the icing period was determined to a high degree of accuracy with this method. Reliable prognoses of ρ_{LWC} will greatly improve the procedures of forecasting duration and intensity of in-cloud icing. Furthermore, testing of this method on similar cases will be necessary in order to verify its accuracy and reliability.

A comparison of measured ice growth rate (kg/s) by the ice scale and estimated ρ_{LWC} (kg/m^3) by use of the lower weather station gave a correlation coefficient of 0.85 for the period identified as in-cloud icing. Based upon this strong correlation a simple model of estimating the coefficient of collision efficiency has been developed. However, further testing of this model is also needed.

A mesoscale model (MM5) was tested at a high horizontal resolution (1km), to evaluate its ability to reproduce weather conditions where freezing occurs. The MM5 forecast identified the start and end times of the icing event with a high degree of accuracy. On the other hand,

the accuracy of the simulated icing intensity was not that good. The MM5 calculations for ice growth gave a value 58% of the actual measured accumulated ice growth. More events of icing should be studied to determine the overall accuracy at a 1 km resolution. However, simulations with the high horizontal resolution used in this case study, are very time consuming. It is not taken for granted that a high resolution forecast would be more accurate than a forecast using a coarser resolution. A study by Mass et al. (2002) shows no increase in accuracy of precipitation when going from 12 to 4 km resolution. Further studies of real-time cases on real-time systems at coarser model resolutions will therefore reveal MM5s capability for making reliable daily forecasts of freezing events.

ACKNOWLEDGEMENTS

REFERENCES

Ahti, K. and Makkonen, L., 1982. Observation on rime formation in relation to routinely measured meteorological parameters, Geophysica, 19(1): 75 – 85.

Bolton, D., 1980. The computation of equivalent potential temperature. Mon. Wea. Rev. 108; 1046 – 1053.

Brun, R. J., Lewis, W., Perkins P. J. and Serafini, J. S., 1955. Impingement of cloud droplets on a cylinder and procedure for measuring liquid-water content and droplet sizes in super cooled clouds by rotating multicylinder method, NACA, Lewis Flight Propulsion Laboratory, Cleveland, Ohio, Rep. No. 1215, 43 pp.

Chaine, P. M. and Skeates, P., 1974. Ice accretion handbook (Freezing Precipitation), Industrial Meteorology Study VI, Environment Canada, Toronto, Canada.

Chang, D., Jiang, L. and Islam, S., 2000. Issues of soil moisture coupling in MM5: Simulation of the diurnal cycle over the FIFE area, J. of Hydromet., 1(6): 477-490.

Chatfield, R., Vastano, J., Li, L., Sachse, G. and Connors, V., 1999. The Great African Plume from biomass burning: generalizations from a three-dimensional study of TRACE A carbon monoxide, J. Geophys. Res., 103(D21): 28059-28077.

Drage, M. A. and de Lange, T., 2004. Description of an ice scale for measuring atmospheric icing. Meteorological report series university of Bergen, 2004. In press.

Eidenshink, J. and Faundeen, J., 1998. The 1-km AVHRR global land dataset: first stages in implementation, Int. J. of Rem. Sens, 15: 3443-3462.

Finstad, K. J. and Lozowski, E. P. and Gates E. M.,1988. A computational investigation of water droplet trajectories, J. Atmos. and Oce, Tech., 5: 160 – 170.

Grell, G., Dudhia, J. and Stauffer, D. 1994. A Description of the Fifth-Generation Penn State/NCAR Mesoscale Model (MM5), NCAR Technical Report Note TN-398, National Center for Atmospheric Research, Boulder Colorado, US.

17

Haldar, A. P., McComber, P., Marshall, M. A., Ichac, M., Goel, A. and Katselein, M., 1996. Validation of ice accretion models for freezing precipitation using filed data, Proceeding 7th International Workshop on Atmospheric Icing of Structures, pp. 189 – 194.

Harstveit, K., 2002. Using routine meteorological data from airfields to produce a map of ice risk zones in Norway. Proceeding 10th International Workshop on Atmospheric Icing of Structures, CD: Session 8-1.

Hong, S. and Pan, H., 1996. Nonlocal Boundary Layer Vertical Diffusion in a Medium Range Forecast Model, Mon. Weather Rev., 124: 2322-2339.

ISO 12494, 2001. ISO (the International Organization for Standardization) 12494 – Atmospheric icing of structures.

Kain, J. S. and Fritsch, J. M., 1993. Convective parameterization for mesoscale models: The Kain-Fritsch scheme. The representation of cumulus convection in numerical models, K. A. Emanuel and D. J. Raymond, Eds., Amer. Meteor. Soc., 246 pp.

Langmuir, I. and Blodgett, K. B., 1946. A mathematical investigation of water droplet trajectories. Collected Works of Irwing Langmuir, Pergamon Press, 10: 348 – 393.

Lott, J. N. and Jones, K. F., 1998. Using U. S. weather data for modeling ice loads from freezing rain, Proceeding 8th International Workshop on Atmospheric Icing of Structures, pp. 157 – 162.

Lozowski, E. P., Stallabras, J. R. and Hearty, P. F., 1983. The icing of an unheated, nonrotating cylinder, Part I: A simulation model, Part II: Icing wind tunnel experiments, J. Climate Appl. Meteor., 22: 2053 -2074.

Ludlam, F. N., 1951. The heat economy of rimed cylinder. Quart. J. Roy. Meteor. Soc., 77: 663 – 666.

Makkonen, L., 1984. Modeling of ice accretion on wires, J. Climate Appl. Meteor., 23: 929 – 939.

Makkonen, L. and Stallabras, J. R., 1987. Experiments on the cloud droplet collision efficiency of cylinders, J. of Clim. Appl. Meteor., 26: 1406 – 1411.

Makkonen, L. and Ahti, K. 1995. Climatic mapping of ice loads based on airport weather observations, Atmos. Res., 36: 185 – 193.

Makkonen, L., 1996. Modeling power line icing in freezing precipitation, Proceeding 7th International Workshop on Atmospheric Icing of Structures, pp. 195 – 200.

Mass, C. and Kuo, Y., 1998. Regional real-time numerical weather prediction: Current status and future potential, Bull. Amer. Meteor. Soc, 79: 253-263.

Mass, C., Ovens, D., Westrick, K. and Colle, B., 2002. Does Increasing horizontal resolution produce more skilful forecasts? Bull. Amer. Meteor. Soc, 83: 407-430.

Mazin, I. P., Korolev, A. V., Heymsfield, A., Isaac, G. A. and Cober, S. G., 2001. Thermodynamics of icing cylinder for measurements of liquid water content in supercooled clouds, J. Atmos. and Oce, Tech., 18: 543 – 558.

Nicholls, S., 1984. The dynamics of stratocumulus: aircraft observations and comparisons with a mixed layer model, Q. J. R. Meteor. Soc., 110: 783 – 820.

Noonkester, V. R., 1984. Droplet spectra observed in marine stratus cloud layers, J. Atmos. Sci., 41: 829 – 845.

Poots, G., 2000. Ice and snow accretion on structures. Phil. Trans. R. Soc. Lond. A (200), 358: 2799 – 3033.

Reisner, J., Rasmussen, R. J. and Bruintjes, R. T., 1998. Explicit forecasting of supercooled liquid water in winter storms using the MM5 mesoscale model, Quart. J. Roy. Meteor. Soc., 124B, 1071-1107.

Rogers, R. R. and Yau, M. K., 1989. A short course in cloud physics, Pergamon Press.

Sundin E. Makkonen L., 1998. Ice loads on a lattice tower estimated by weather station data. J. Appl. Meteoror. Vol. 37, pp. 523-529.

Vassbø, T., Kristjansson, J. E., Fikke, S. M. and Makkonen, L., 1998. An Investigation of the Feasibility of Predicting Icing Episodes using Numerical Weather Prediction Model Output. Proceeding 8th International Workshop on Atmospheric Icing of Structures.

Warner, T., Kibler, D. and Steinhart, R., 1991. Separate and coupled testing of meteorological and hydrological forecast models for the Susquehanna River Basin in Pennsylvania, J. Appl. Meteor., 30: 1521-1533.

Warner, T., Peterson, R. A. and Treadon, R. E., 1998. A tutorial on lateral boundary conditions as a basic and potential serious limitation to regional numerical weather prediction, Bull. Amer. Meteor. Soc, 78: 2599-2617.